Letter

Large kagome family candidates with topological superconductivity and charge density waves

Xin-Wei Yi,[1] Xing-Yu Ma,[1] Zhen Zhang,[1] Zheng-Wei Liao,[1] Jing-Yang You,[2,*] and Gang Su[1,3,†]

[1]*School of Physical Sciences, University of Chinese Academy of Sciences, Beijing 100049, China*

[2]*Department of Physics, Faculty of Science, National University of Singapore, 117551 Singapore*

[3]*Kavli Institute for Theoretical Sciences, and CAS Center for Excellence in Topological Quantum Computation, University of Chinese Academy of Sciences, Beijing 100190, China*

(Received 30 January 2022; revised 22 November 2022; accepted 13 December 2022; published 27 December 2022)

A group of recently discovered nonmagnetic metal kagome structures AV_3Sb_5 (A = K, Rb, Cs) has aroused widespread interest both experimentally and theoretically due to their unusual charge density wave (CDW) and intertwined superconductivity. However, they all possess weak electron-phonon coupling (EPC) and low superconducting transition temperature T_c. Here, we perform high-throughput first-principles calculations on such kagome candidates with AV_3Sb_5 prototype structure, and propose 24 dynamically stable kagome metals. The calculation based on Bardeen-Cooper-Schrieffer theory shows that most of these metals are superconductors with much stronger EPC than the reported AV_3Sb_5 materials, and their T_c are between 0.3 and 5.0 K. Moreover, several compounds, such as KZr_3Pb_5 with the highest T_c, are identified as $\mathbb{Z}_2$ topological metals with clear Dirac cone topological surface states near the Fermi level. In addition, we take $NaZr_3As_5$ as an example to demonstrate the possible CDW phases. Our results provide rich platforms for exploring various physics with the kagome structure, in which the coexistence of superconductivity and the nontrivial topological nature provides promising insights for the discovery of topological superconductors.

DOI: 10.1103/PhysRevB.106.L220505

Introduction. In 2019, a group of nonmagnetic metals AV_3Sb_5 (A = K, Rb, and Cs) with perfect vanadium kagome net was synthesized [1]. Since then, surprises have emerged in the study of these structures. The electronic structures of AV_3Sb_5 show Dirac nodal lines, nontrivial $\mathbb{Z}_2$ topological band index, and clear topological surface states near the Fermi level, indicating that their normal states are $\mathbb{Z}_2$ topological metals [1–4]. The superconducting transition temperatures T_c of AV_3Sb_5 (A = K, Rb, and Cs) are 0.93 [2], 0.92 [5], and 2.5 K [3] (2.3 K [6,7]), respectively, and the temperatures T^* corresponding to the charge density wave (CDW) transition are 78 [8], 102 [9], and 94 K [10], respectively. The exotic CDW states of the non-electron-phonon coupling (non-EPC) mechanism [9] display many unconventional characteristics. The CDWs in these three compounds exhibit chiral anisotropy [11–13] and reduce the density of electronic states near the Fermi level [11,14–16]. Various evidence, including giant anomalous Hall response [17,18], CDW chirality adjustable by magnetic field [11–13], edge supercurrent [19], and spontaneous internal magnetic field [20], indicate that the charge order may break the time-reversal symmetry, which has also been verified theoretically [11,21,22]. Moreover, CsV_3Sb_5 samples have been found to own roton pair density wave [7], which is similar to the one in unconventional high-T_c cuprate superconductors [23]. The coexistence of V- and U-shaped superconducting gaps [24] and the anisotropic superconducting properties in CsV_3Sb_5 [25] imply the possible multiband superconducting pairing. Intertwined superconductivity with CDW shows many different features. For instance, T_c exhibits an unconventional double dome behavior, and T^* decreases rapidly with increasing pressure [8,10,26]. The second dome of T_c and the disappearance of T^* occur at the same pressure. The superconducting properties and charge order of AV_3Sb_5 can also be tuned by magnetic impurity [24], strain [27], and thickness [28–30], which dramatically enrich the phase diagram. The experimental and theoretical studies of AV_3Sb_5 show a complementary and rapid trend. However, AV_3Sb_5 all display weak EPC and low superconducting T_c, and finding more potential compounds with higher T_c from the prototype structure of AV_3Sb_5 is desirable. In addition, as topological superconductors in experiments are extremely rare, discovering more materials combining nontrivial topological surface states near the Fermi level and high-T_c superconductivity will provide rich platforms for the discovery of topological superconductivity and Majorana zero modes [31–36].

In this Letter, we first apply the high-throughput first-principles calculations to 800 new kagome structures based on the AV_3Sb_5 prototype structure, and find 24 dynamically stable metal compounds. Then, we carefully study their superconducting and topological properties. The results show that 14 compounds are superconductors with a T_c between 0.3 and 5.0 K. Moreover, several structures, including KZr_3Pb_5 with the highest T_c, have strong $\mathbb{Z}_2$ indices with abundant nontrivial topological surface states near the Fermi surface, suggesting that they are $\mathbb{Z}_2$ topological metals. The coexistence of superconductivity and nontrivial band topology opens a door for the discovery of topological superconductivity based on the kagome net. Additionally,

*phyjyy@nus.edu.sg
†gsu@ucas.ac.cn

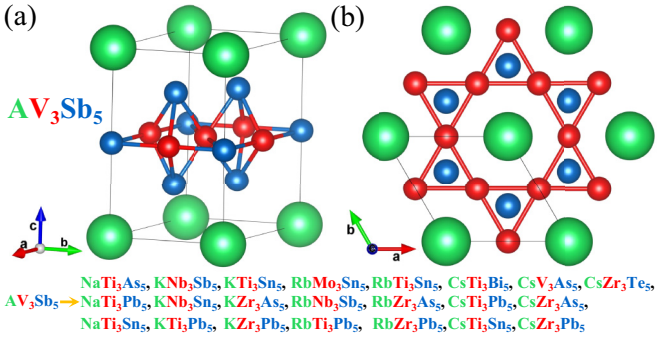

FIG. 1. The crystal structure of AV_3Sb_5, where 22 new stable AB_3C_5 members with the same crystal structure as AV_3Sb_5 are indicated.

we also find two possible CDW phases in $NaZr_3As_5$, which may provide useful information for further understanding the CDW phases in AV_3Sb_5.

Crystal structure of AV_3Sb_5. The AV_3Sb_5 crystallize in a layered structure with the space group of P6/mmm (No. 191) as shown in Fig. 1. The perfect V-kagome net mixed with the Sb-triangular net is located in the middle layer, which is sandwiched by two additional Sb honeycomb layers. The upper and lower triangular layers of alkali-metal A atoms have a large bond distance relative to the middle V-Sb layer and are thus loosely bonded to them.

Searching new structures. The high-throughput first-principles calculations are used to search for kagome topological superconductor candidates (as indicated in Fig. S1 in the Supplemental Material (SM) [37]). Based on the prototype structure of AV_3Sb_5, 800 compounds are constructed by replacing A with alkali-metal elements Li, Na, K, Rb, and Cs, replacing V with all transition-metal elements in the fourth and fifth periods of the periodic table, and replacing Sb with its neighboring elements (Ge, As, Se, Sn, Sb, Te, Pb, and Bi). These compounds will be abbreviated as AB_3C_5 below. For all these compounds, we first carry out fully geometric relaxation in magnetic configurations (see Fig. S2 in the SM [37]). Then, by comparing the total energies of magnetic configurations, each AB_3C_5 member can be classified as nonmagnet (NM), ferromagnet (FM), and antiferromagnet (AFM). Phonon spectra are calculated to determine the dynamic stability of these AB_3C_5 members. Those compounds without imaginary frequency in the phonon spectra will be further analyzed for their corresponding electronic structures, superconductivity, and topological properties. On the other hand, compounds with imaginary phonon frequency will be used to discuss possible CDW phases.

In doing so, we discover 24 new stable AB_3C_5 members, including 22 NM, one FM, and one AFM, and their lattice information is listed in Table S1 in the SM [37]. The spin-polarized calculations show that $CsTi_3Pb_5$ has a ferromagnetic ground state with magnetic easy-axis anisotropy and the magnetocrystalline anisotropy energy is -1.59 meV/f.u. $RbCr_3Te_5$ has an in-plane 120° AFM ground state. The Monte Carlo simulations estimate that the Curie temperature of $CsTi_3Pb_5$ is about 18 K, and the Neel temperature of $RbCr_3Te_5$ is about 13 K. In addition, the formation energies

TABLE I. Electronic density of states per formula unit at Fermi energy $N(E_F)$ (eV^{-1} f.u.$^{-1}$), logarithmic average frequency ω_{log} (K), EPC $\lambda(\omega=\infty)$, and T_c of 14 stable compounds.

	$N(E_F)$ (eV^{-1} f.u.$^{-1}$)	ω_{log} (K)	λ	T_c (K)
KNb_3Sn_5	4.22	149.1	0.52	2.102
$CsRu_3Ge_5$	3.19	170.8	0.36	0.353
$RbTi_3Bi_5$	5.96	149.8	0.41	0.719
$CsTi_3Bi_5$	5.96	163.4	0.35	0.316
KTi_3Pb_5	7.29	157.9	0.51	2.039
$RbTi_3Pb_5$	7.50	156.5	0.50	1.857
KTi_3Sn_5	6.57	180.3	0.42	0.974
$RbTi_3Sn_5$	6.50	182.5	0.42	0.961
$CsTi_3Sn_5$	6.87	174.6	0.45	1.375
$CsZr_3As_5$	3.40	125.8	0.56	2.289
KZr_3Pb_5	6.47	94.1	0.91	5.027
$RbZr_3Pb_5$	6.56	111.9	0.72	4.154
$CsZr_3Pb_5$	6.53	119.2	0.58	2.438
$CsZr_3Te_5$	2.88	123.5	0.48	1.266

are calculated to further demonstrate their stabilities, as listed in Table S1 in the SM [37]. Electronic structure calculations show that they are all metals similar to AV_3Sb_5. Furthermore, 22 members maintain the same crystal structure as AV_3Sb_5 after structural optimization (as listed in Fig. 1), except for $CsRu_3Ge_5$ and $RbCr_3Te_5$, whose triangles in the kagome nets are twisted, changing their space group to $P\bar{6}2m$.

Superconductivity. The metallicity of these 24 AB_3C_5 members enables us to perform further calculations on superconductivity. We calculate the Eliashberg spectral function $\alpha^2F(\omega)$ and cumulative EPC $\lambda(\omega)$ of these materials at ambient pressure, and estimate the T_c with the McMillan-Allen-Dynes approach of Bardeen-Cooper-Schrieffer (BCS) theory (see the SM for details [37]). After careful calculations and screening, we find that 14 of these 24 members have the superconducting ground state as listed in Table I, where KZr_3Pb_5 possesses the highest T_c of 5.027 K, which is more than twice the experimental values of AV_3Sb_5 (see Table II) [2,3,5–7].

We choose the AZr_3Pb_5 group with relatively higher T_c for further discussions. Their phonon spectra, phonon density of states (PhDOS), $\alpha^2F(\omega)$, and $\lambda(\omega)$ are plotted in Fig. 2. We can see that the phonon spectra of the three compounds are very similar. A careful comparison of their phonon spectra shows that the faint phonon softening at the L point gradually becomes obvious from K to Rb to Cs. It can be seen from PhDOS that the contributions of the Pb and Zr atoms

TABLE II. Electronic density of states at the Fermi energy $N(E_F)$ (eV^{-1} f.u.$^{-1}$), EPC $\lambda(\omega=\infty)$, calculated T_c, and experimental superconducting temperature T_c^{exp} for the inverse Star of David (ISD) phase of AV_3Sb_5 [2,3,5–7,38] and pristine phase of AZr_3Pb_5.

	$N(E_F)$ (eV^{-1} f.u.$^{-1}$)	λ	T_c (K)	T_c^{exp} (K)
KV_3Sb_5	2.9	0.38	0.22	0.93
RbV_3Sb_5	2.33	0.32	0.05	0.92
CsV_3Sb_5	1.30	0.25	0.0008	2.5(2.3)

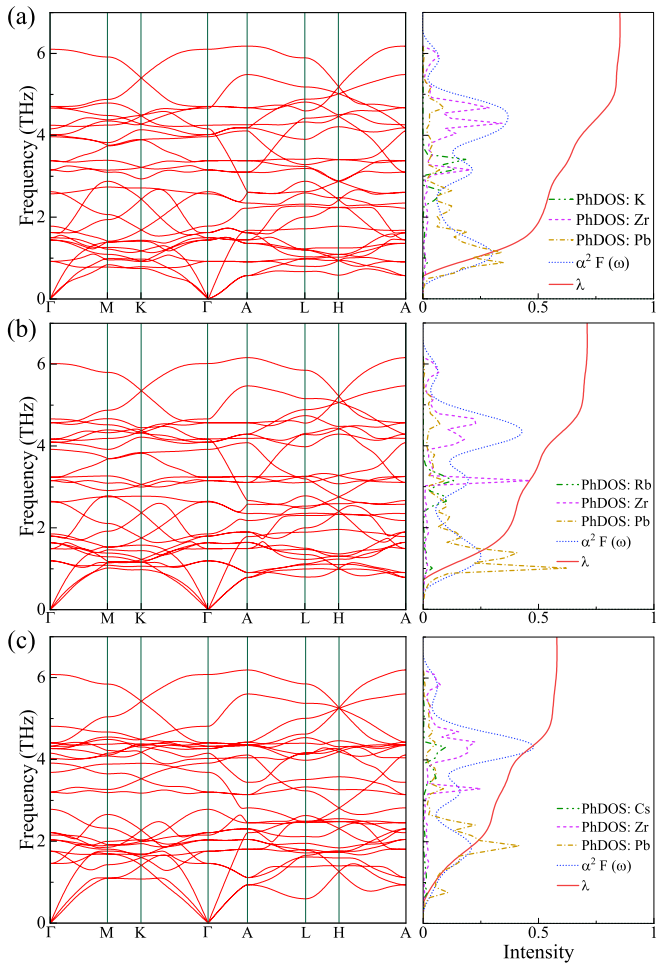

FIG. 2. The phonon spectra, projected PhDOS, Eliashberg spectral function $\alpha^2F(\omega)$, and cumulative frequency-dependent EPC $\lambda(\omega)$ of (a) KZr_3Pb_5, (b) $RbZr_3Pb_5$, and (c) $CsZr_3Pb_5$.

to PhDOS are mainly distributed in the relatively low- and high-frequency regions with several prominent peaks, respectively, while the PhDOS of alkali-metal atoms distributed in the medium-frequency region are very small. The relatively low-frequency (<3 THz) phonons corresponding to the vibration modes of Pb account for more than half of the total EPC. The T_c of the three compounds decreases with the gradual increase of the atomic number of alkali metals, as shown in Table I. The gradual decrease of T_c from K to Rb to Cs is due to the negligible contribution of alkali-metal elements to the EPC, and the increase of atomic radius from K to Cs, resulting in the gradual increase of the lattice parameters, is equivalent to applying a negative pressure (tensile strain) to the lattice, which significantly reduce the parameters related to the lattice and weaken the EPC.

Electronic band structure and topological property. We plot the electronic energy bands and density of states (DOS) with spin-orbit coupling (SOC) for KZr_3Pb_5 in Fig. 3(a). The electronic band structures of $RbZr_3Pb_5$ and $CsZr_3Pb_5$ are also given in Figs. S24 and S25 in the SM [37]. The 3D Fermi surface (FS) of KZr_3Pb_5 and its 2D slice at the $k_z = 0$ and π planes are drawn in Figs. 3(b)–3(d), which is obviously different from the FS of AV_3Sb_5 that exhibits strong 2D characteristics. Furthermore, we can see the obvious Fermi surface nesting with the nesting vector parallel to *A*-*L* and *A*-*H* in the $k_z = \pi$ slice.

AZr_3Pb_5 are nonmagnetic, similar to AV_3Sb_5. Therefore, combining the time-reversal and inversion symmetries of AZr_3Pb_5, we can get their $\mathbb{Z}_2$ topological invariant by calculating the parity of the wave functions at all time-reversal invariant momenta (TRIM) points [39]. It can be seen from Fig. 3(e) that all the energy bands passing through the Fermi surface have a strong topological $\mathbb{Z}_2$ index, resulting in abundant Dirac cone surface states near the Fermi level, as shown in Figs. 3(g) and 3(h). The continuous band gap between adjacent energy bands near the Fermi level, as shaded in Fig. 3(a), nontrivial topological surface states, and strong $\mathbb{Z}_2$ index of bands near the Fermi level make KZr_3Pb_5 a $\mathbb{Z}_2$ topological metal. Similar analysis shows that many other AB_3C_5 members, such as $CsZr_3Pb_5$, are also $\mathbb{Z}_2$ topological metals.

Possible CDW phases. We take $NaZr_3As_5$ as an example to explore the possible CDW phases. One may find that the phonon spectrum in Fig. 4(d) shows obvious softening acoustic phonon modes at the *M* and *L* points at the boundaries of the Brillouin zone, and the imaginary frequency at the *L* point is slightly larger than that at the *M* point, which is very similar to AV_3Sb_5 [15,38]. The symmetry analysis on AV_3Sb_5 indicates that the irreducible representations of the imaginary mode at the *M* and *L* points are M_1^+ and L_2^-, respectively, which is also consistent with the previous studies [15,40]. However, similar analysis shows that the irreducible representations of the imaginary mode in $NaZr_3As_5$ are M_2^+ and L_1^-, which makes $NaZr_3As_5$ exhibit completely different distortions from AV_3Sb_5. In consideration of one *L* point, it gives the phase as shown in Fig. 4(b). The soft mode at the *M* point makes corner-shared triangles in layers rotate around the corner, while the soft mode at the *L* point leads to the distortion of adjacent layers with an additional π shift. Clockwise and counterclockwise distortions will generate the same structure. The combination of all three unequal *L* points gives a similar phase as shown in Fig. 4(c), which differs from Fig. 4(b) in that Zr atoms in the kagome layers rotate around the center of the triangles. These two structures have *Ibam* (No. 72) and *P*6/*mcc* (No. 192) space groups, respectively. Both of them reduce the rotation symmetry of C_6 to C_2, but still retain the spatial inversion symmetry.

Their phonon spectra in Figs. 4(e) and 4(f) show dynamic stability without imaginary frequency, so both of them are possible CDW phases of $NaZr_3As_5$. We label them CDW I and CDW II, respectively. Compared with the pristine phase, the displacement values of Zr atoms in the kagome layer in CDW I and CDW II are 0.12 and 0.15 Å, respectively. The total energy as a function of the displacement of Zr atoms is shown in Figs. 4(h) and 4(i). The total energies of the two stable CDW phases are 11.3 and 25.1 meV/cell lower than that of a pristine structure, respectively.

The unfolded energy bands and DOS of the CDW phases in Fig. S31 (see the SM [37]) show no obvious change compared with the pristine phase, except that some gaps are opened and the saddle point at the *L* point moves closer to the Fermi level. Saddle-point nesting in the electronic structure is unlikely the origin of the CDW order in $NaZr_3As_5$. The real CDW phase, its origin, and the possible interplay between charge order and

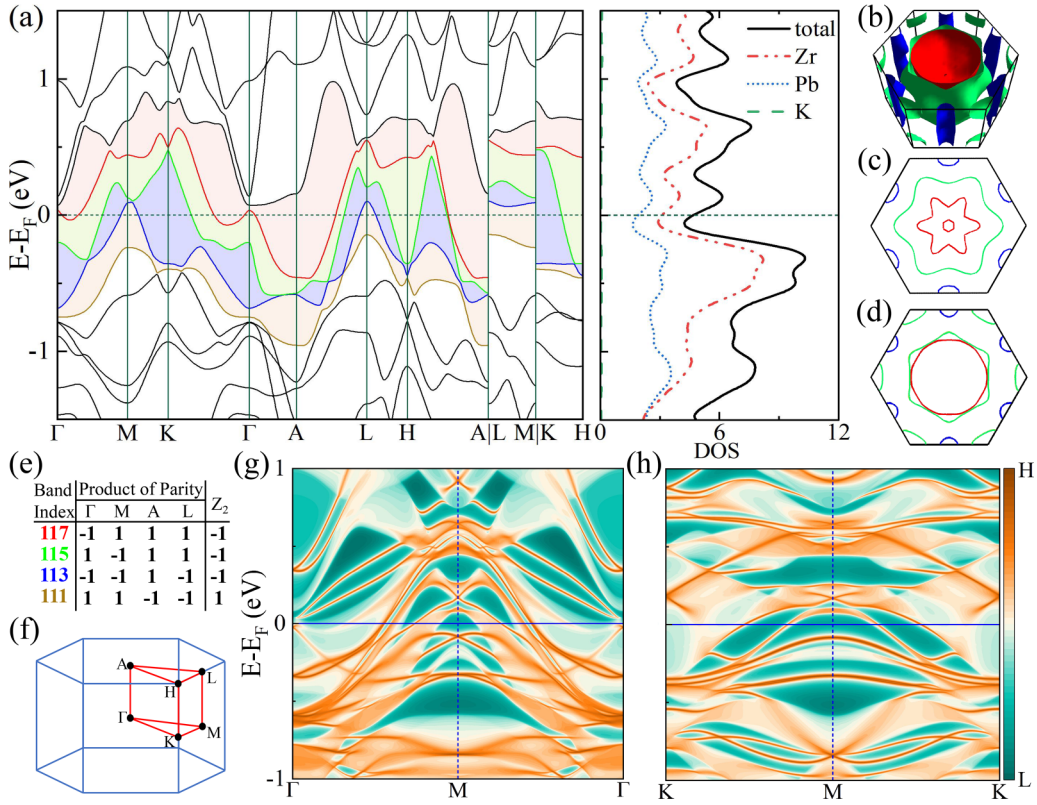

FIG. 3. (a) The electronic energy bands and density of states calculated with SOC for KZr_3Pb_5. The continuous direct gap between adjacent energy bands is shaded. (b) Three-dimensional (3D) FS of KZr_3Pb_5 and its 2D maps at (c) $k_z = 0$ and (d) π slices. Different colors of FS refer to different band indices consistent with (a). (e) Product of parity and $\mathbb{Z}_2$ indices of bands near the Fermi level. (f) The Brillouin zone with high-symmetry paths indicated. Topological surface states along (g) Γ-*M*-Γ and (h) *K*-*M*-*K* paths on the (001) plane for KZr_3Pb_5.

superconductivity in $NaZr_3As_5$ deserve future experimental exploration. Besides $NaZr_3As_5$, we also plot those structures with obvious soft modes at high-symmetry paths that may have CDW phases, in Fig. S32 of the SM [37].

Discussion. In addition to AZr_3Pb_5, the calculated results of all other stable AB_3C_5 members are presented in Figs. S3–S23 in the SM [37]. The new AV_3C_5 members are not only structurally similar to AV_3Sb_5, but also inherit many attractive features, such as Van Hove singularities, Dirac points, Dirac nodal lines, and strong 2D characteristics of the phonon spectrum and FS, which are worthy of further studies.

For all AB_3C_5 kagome families proposed in this Letter and the reported AV_3Sb_5, we hardly see some obvious flat bands in the band structures. To further interpret this feature, we construct a tight-binding model in the SM [37]. By tuning the hopping parameters, we find that with the increase of the hopping parameters between the B atoms of the kagome lattice and C atoms, the flat band becomes more dispersive, as seen in Fig. S27 in the SM [37]. The C atoms and kagome B atoms are very close to each other, and the overlap of their orbitals makes the interaction between them very complex and destroys the destructive interference condition for the formation of a flat band in the kagome lattice, resulting in the disappearance of the flat band.

An important feature of those predicted structures beyond AV_3Sb_5 is their much stronger EPC strength. The calculated T_c of KV_3Sb_5, RbV_3Sb_5, and CsV_3Sb_5 based on BCS theory are 0.0008, 0.05, and 0.22 K, respectively [38], which are much lower than their experimental values (see Table II), because the CDW in AV_3Sb_5 reduces the DOS near the Fermi level and suppresses the BCS superconductivity. This indicates there may be an unconventional superconducting mechanism. This mechanism is also expected to appear in the materials listed in Table I. From Tables I and II, it can be observed that the calculated T_c of AZr_3Pb_5 are much higher than those of AV_3Sb_5, thereby experimental T_c of AZr_3Pb_5 may be higher.

The coexistence of superconductivity and topological nontrivial surface states is essentially rare [41–45]. It is reported that the robust zero-bias conductance peak in CsV_3Sb_5 exhibits similar characteristics to the $Bi_2Te_3/NbSe_2$ heterostructures with Majorana bound state [6]. Our proposed compounds with both the superconducting ground state and the nontrivial topological surface states near the Fermi level would provide a rich platform for exploring topological superconductivity and Majorana zero-energy modes.

Mature experimental methods such as the flux method have been used to synthesize high-quality and stable AV_3Sb_5 compounds, which is a prerequisite for the rapid development of experimental analysis. In the initial work of Brenden *et al.* for the AV_3Sb_5 family, they explore the combination of (K, Rb, Cs)(V, Nb, Ta)(Sb, Bi) under different synthetic conditions [1]. However, only KV_3Sb_5, RbV_3Sb_5, and CsV_3Sb_5 are crystallized. In this work, 800 AB_3C_5 members in the high-throughput screening process contain most of the combinations they explored. Our calculation results show that those

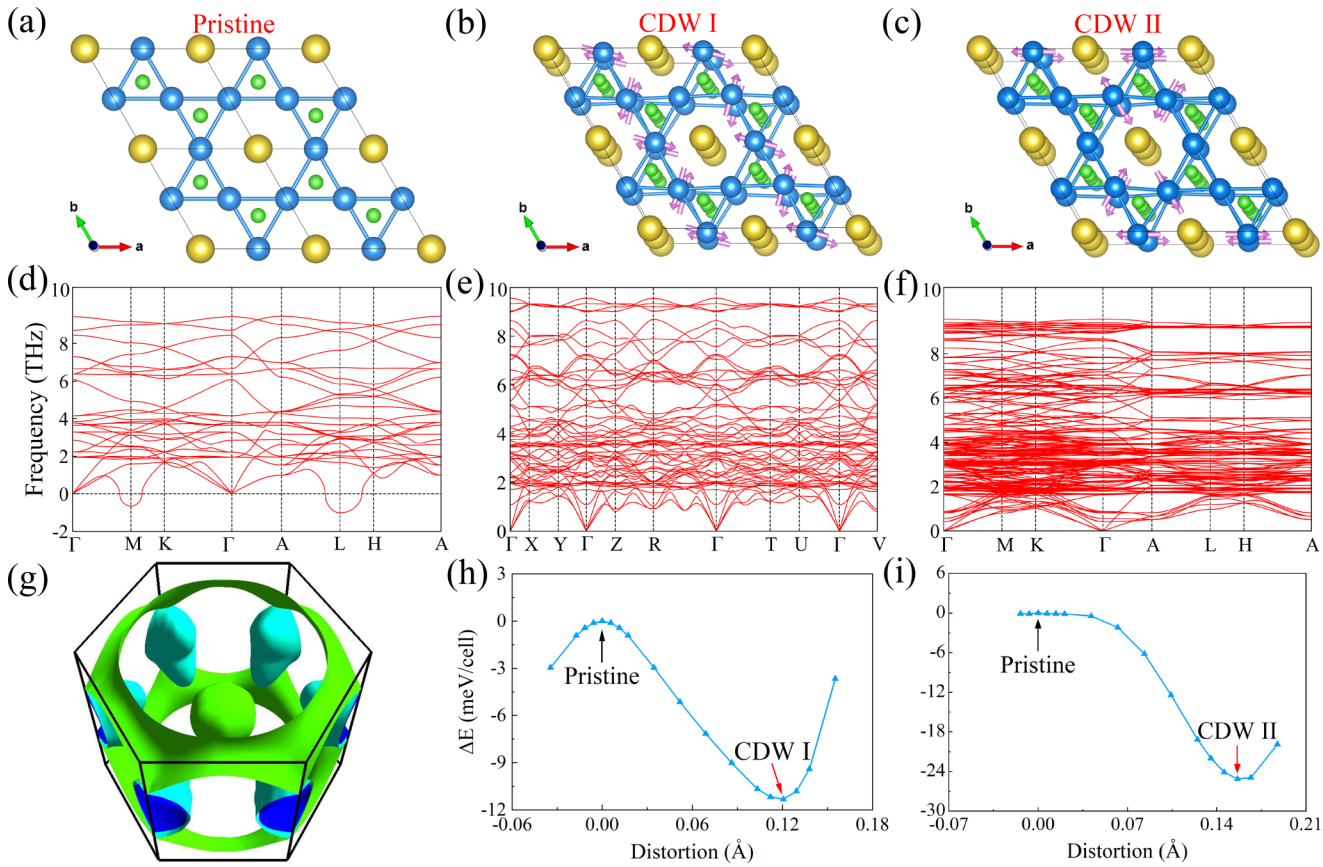

FIG. 4. Crystal structures of $NaZr_3As_5$ in the (a) 2×2 supercell of pristine phase, (b) CDW I phase, and (c) the CDW II phase and their corresponding phonon spectra (d)–(f), respectively. (g) 3D FS of $NaZr_3As_5$. The comparison of total energies ΔE for (h) pristine phase and CDW I, and (i) pristine phase and CDW II, where the distortion represents the displacement of Zr atoms and ΔE stands for the relative total energy with respect to the pristine phase per cell with 72 atoms. The Brillouin zone of (b) and high-symmetry paths of (e) are plotted in Fig. S31(d) in the SM [37].

compounds that were not synthesized in their experiment are dynamically unstable, except KNb_3Sb_5. The good agreement with the experimental results indicates that our present calculations are reasonable, and the stable structures presented here are very likely to be synthesized in future experiments. Very recently, another family of kagome metals RV_6Sn_6 (R = Gd, Ho, Y) with two V-derived kagome layers in the primitive cell were also synthesized by the flux method [46,47]. Therefore, the versatile and matured flux method may be employed to synthesize the stable structures in Table S1 in the SM [37].

Summary. In conclusion, we calculate 800 kagome candidates based on the prototype structure of AV_3Sb_5 using a high-throughput density functional theory (DFT) screening process, and discover 24 dynamically stable metal compounds, including one ferromagnetic, one antiferromagnetic, and 22 nonmagnetic structures. These compounds display many appealing properties similar to AV_3Sb_5. Furthermore, 14 compounds among them are predicted to be phonon-mediated BCS superconductors with T_c between 0.316 and 5.027 K. KZr_3Pb_5 with the highest T_c exhibits a strong $\mathbb{Z}_2$ invariant of the energy bands and abundant nontrivial topological surface states near the Fermi level, revealing a $\mathbb{Z}_2$ topological metal. In addition, we also find two possible CDW phases in $NaZr_3As_5$. This present work would give more insights into the exploration of possible topological superconductors.

Acknowledgments. This work is supported in part by the National Key R&D Program of China (Grant No. 2018YFA0305800), the Strategic Priority Research Program of the Chinese Academy of Sciences (Grant No. XDB28000000), the National Natural Science Foundation of China (Grant No.11834014), and the High-magnetic Field Center of the Chinese Academy of Sciences.

[1] B. R. Ortiz, L. C. Gomes, J. R. Morey, M. Winiarski, M. Bordelon, J. S. Mangum, I. W. H. Oswald, J. A. Rodriguez-Rivera, J. R. Neilson, S. D. Wilson, E. Ertekin, T. M. McQueen, and E. S. Toberer, New kagome prototype materials: Discovery of KV_3Sb_5, RbV_3Sb_5, and CsV_3Sb_5, Phys. Rev. Mater. **3**, 094407 (2019).

[2] B. R. Ortiz, P. M. Sarte, E. M. Kenney, M. J. Graf, S. M. L. Teicher, R. Seshadri, and S. D. Wilson, Superconductivity in

the Z_2 kagome metal KV_3Sb_5, Phys. Rev. Mater. **5**, 034801 (2021).

[3] B. R. Ortiz, S. M. L. Teicher, Y. Hu, J. L. Zuo, P. M. Sarte, E. C. Schueller, A. M. Milinda Abeykoon, M. J. Krogstad, S. Rosenkranz, R. Osborn, R. Seshadri, L. Balents, J. He, and S. D. Wilson, CsV_3Sb_5 : A Z_2 Topological Kagome Metal with a Superconducting Ground State, Phys. Rev. Lett. **125**, 247002 (2020).

[4] J. Zhao, W. Wu, Y. Wang, and S. A. Yang, Electronic correlations in the normal state of the kagome superconductor KV_3Sb_5, Phys. Rev. B **103**, L241117 (2021).

[5] Q. Yin, Z. Tu, C. Gong, Y. Fu, S. Yan, and H. Lei, Superconductivity and normal-state properties of kagome metal RbV_3Sb_5 single crystals, Chin. Phys. Lett. **38**, 037403 (2021).

[6] Z. Liang, X. Hou, F. Zhang, W. Ma, P. Wu, Z. Zhang, F. Yu, J.-J. Ying, K. Jiang, L. Shan, Z. Wang, and X.-H. Chen, Three-dimensional Charge Density Wave and Surface-Dependent Vortex-Core States in a Kagome Superconductor CsV_3Sb_5, Phys. Rev. X **11**, 031026 (2021).

[7] H. Chen, H. Yang, B. Hu, Z. Zhao, J. Yuan, Y. Xing, G. Qian, Z. Huang, G. Li, Y. Ye, S. Ma, S. Ni, H. Zhang, Q. Yin, C. Gong, Z. Tu, H. Lei, H. Tan, S. Zhou, C. Shen *et al.*, Roton pair density wave in a strong-coupling kagome superconductor, Nature (London) **599**, 222 (2021).

[8] F. Du, S. Luo, B. R. Ortiz, Y. Chen, W. Duan, D. Zhang, X. Lu, S. D. Wilson, Y. Song, and H. Yuan, Pressure-induced double superconducting domes and charge instability in the kagome metal KV_3Sb_5, Phys. Rev. B **103**, L220504 (2021).

[9] H. Li, T. T. Zhang, T. Yilmaz, Y. Y. Pai, C. E. Marvinney, A. Said, Q. W. Yin, C. S. Gong, Z. J. Tu, E. Vescovo, C. S. Nelson, R. G. Moore, S. Murakami, H. C. Lei, H. N. Lee, B. J. Lawrie, and H. Miao, Observation of Unconventional Charge Density Wave Without Acoustic Phonon Anomaly in Kagome Superconductors AV_3Sb_5 (A = Rb, Cs), Phys. Rev. X **11**, 031050 (2021).

[10] K. Y. Chen, N. N. Wang, Q. W. Yin, Y. H. Gu, K. Jiang, Z. J. Tu, C. S. Gong, Y. Uwatoko, J. P. Sun, H. C. Lei, J. P. Hu, and J.-G. Cheng, Double Superconducting Dome and Triple Enhancement of T_c in the Kagome Superconductor CsV_3Sb_5 Under High Pressure, Phys. Rev. Lett. **126**, 247001 (2021).

[11] Y.-X. Jiang, J.-X. Yin, M. M. Denner, N. Shumiya, B. R. Ortiz, G. Xu, Z. Guguchia, J. He, M. S. Hossain, X. Liu, J. Ruff, L. Kautzsch, S. S. Zhang, G. Chang, I. Belopolski, Q. Zhang, T. A. Cochran, D. Multer, M. Litskevich, Z.-J. Cheng *et al.*, Unconventional chiral charge order in kagome superconductor KV_3Sb_5, Nat. Mater. **20**, 1353 (2021).

[12] Z. Wang, Y.-X. Jiang, J.-X. Yin, Y. Li, G.-Y. Wang, H.-L. Huang, S. Shao, J. Liu, P. Zhu, N. Shumiya, M. S. Hossain, H. Liu, Y. Shi, J. Duan, X. Li, G. Chang, P. Dai, Z. Ye, G. Xu, Y. Wang *et al.*, Electronic nature of chiral charge order in the kagome superconductor CsV_3Sb_5, Phys. Rev. B **104**, 075148 (2021).

[13] N. Shumiya, M. S. Hossain, J.-X. Yin, Y.-X. Jiang, B. R. Ortiz, H. Liu, Y. Shi, Q. Yin, H. Lei, S. S. Zhang, G. Chang, Q. Zhang, T. A. Cochran, D. Multer, M. Litskevich, Z.-J. Cheng, X. P. Yang, Z. Guguchia, S. D. Wilson, and M. Z. Hasan, Intrinsic nature of chiral charge order in the kagome superconductor RbV_3Sb_5, Phys. Rev. B **104**, 035131 (2021).

[14] E. Uykur, B. R. Ortiz, S. D. Wilson, M. Dressel, and A. A. Tsirlin, Optical detection of the density-wave instability in the kagome metal KV_3Sb_5, npj Quantum Mater. **7**, 16 (2022).

[15] N. Ratcliff, L. Hallett, B. R. Ortiz, S. D. Wilson, and J. W. Harter, Coherent phonon spectroscopy and interlayer modulation of charge density wave order in the kagome metal CsV_3Sb_5, Phys. Rev. Mater. **5**, L111801 (2021).

[16] S. Cho, H. Ma, W. Xia, Y. Yang, Z. Liu, Z. Huang, Z. Jiang, X. Lu, J. Liu, Z. Liu, J. Li, J. Wang, Y. Liu, J. Jia, Y. Guo, J. Liu, and D. Shen, Emergence of New Van Hove Singularities in the Charge Density Wave State of a Topological Kagome Metal RbV_3Sb_5, Phys. Rev. Lett. **127**, 236401 (2021).

[17] F. H. Yu, T. Wu, Z. Y. Wang, B. Lei, W. Z. Zhuo, J. J. Ying, and X. H. Chen, Concurrence of anomalous Hall effect and charge density wave in a superconducting topological kagome metal, Phys. Rev. B **104**, L041103 (2021).

[18] S.-Y. Yang, Y. Wang, B. R. Ortiz, D. Liu, J. Gayles, E. Derunova, R. Gonzalez-Hernandez, L. Šmejkal, Y. Chen, S. S. P. Parkin, S. D. Wilson, E. S. Toberer, T. McQueen, and M. N. Ali, Giant, unconventional anomalous Hall effect in the metallic frustrated magnet candidate, KV_3Sb_5, Sci. Adv. **6**, eabb6003 (2020).

[19] Y. Wang, S. Yang, P. K. Sivakumar, B. R. Ortiz, S. M. L. Teicher, H. Wu, A. K. Srivastava, C. Garg, D. Liu, S. S. P. Parkin, E. S. Toberer, T. McQueen, S. D. Wilson, and M. N. Ali, Proximity-induced spin-triplet superconductivity and edge supercurrent in the topological kagome metal, $K_{1-x}V_3Sb_5$, arXiv:2012.05898.

[20] C. Mielke III, D. Das, J.-X. Yin, H. Liu, R. Gupta, Y.-X. Jiang, M. Medarde, X. Wu, H. C. Lei, J. Chang, P. Dai, Q. Si, H. Miao, R. Thomale, T. Neupert, Y. Shi, R. Khasanov, M. Z. Hasan, H. Luetkens, and Z. Guguchia, Time-reversal symmetry-breaking charge order in a kagome superconductor, Nature (London) **602**, 245 (2022).

[21] M. M. Denner, R. Thomale, and T. Neupert, Analysis oF Charge Order in the Kagome Metal AV_3Sb_5 (A = K, Rb, Cs), Phys. Rev. Lett. **127**, 217601 (2021).

[22] Y.-P. Lin and R. M. Nandkishore, Complex charge density waves at Van Hove singularity on hexagonal lattices: Haldane-model phase diagram and potential realization in the kagome metals AV_3Sb_5 (A = K, Rb, Cs), Phys. Rev. B **104**, 045122 (2021).

[23] W. Ruan, X. Li, C. Hu, Z. Hao, H. Li, P. Cai, X. Zhou, D.-H. Lee, and Y. Wang, Visualization of the periodic modulation of Cooper pairing in a cuprate superconductor, Nat. Phys. **14**, 1178 (2018).

[24] H.-S. Xu, Y.-J. Yan, R. Yin, W. Xia, S. Fang, Z. Chen, Y. Li, W. Yang, Y. Guo, and D.-L. Feng, Multiband Superconductivity with Sign-Preserving Order Parameter in Kagome Superconductor CsV_3Sb_5, Phys. Rev. Lett. **127**, 187004 (2021).

[25] S. Ni, S. Ma, Y. Zhang, J. Yuan, H. Yang, Z. Lu, N. Wang, J. Sun, Z. Zhao, D. Li, S. Liu, H. Zhang, H. Chen, K. Jin, J. Cheng, L. Yu, F. Zhou, X. Dong, J. Hu, H.-J. Gao *et al.*, Anisotropic superconducting properties of kagome metal CsV_3Sb_5, Chin. Phys. Lett. **38**, 057403 (2021).

[26] F. H. Yu, D. H. Ma, W. Z. Zhuo, S. Q. Liu, X. K. Wen, B. Lei, J. J. Ying, and X. H. Chen, Unusual competition of superconductivity and charge-density-wave state in a compressed topological kagome metal, Nat. Commun. **12**, 23928 (2021).

[27] L. Yin, D. Zhang, C. Chen, G. Ye, F. Yu, B. R. Ortiz, S. Luo, W. Duan, H. Su, J. Ying, S. D. Wilson, X. Chen, H. Yuan, Y. Song, and X. Lu, Strain-sensitive superconductivity in the kagome metals KV_3 Sb_5 and CsV_3 Sb_5 probed by point-contact spectroscopy, Phys. Rev. B **104**, 174507 (2021).

[28] T. Wang, A. Yu, H. Zhang, Y. Liu, W. Li, W. Peng, Z. Di, D. Jiang, and G. Mu, Enhancement of the superconductivity and quantum metallic state in the thin film of superconducting kagome metal KV_3 Sb_5, arXiv:2105.07732.

[29] B. Q. Song, X. M. Kong, W. Xia, Q. W. Yin, C. P. Tu, C. C. Zhao, D. Z. Dai, K. Meng, Z. C. Tao, Z. J. Tu, C. S. Gong, H. C. Lei, Y. F. Guo, X. F. Yang, and S. Y. Li, Competing superconductivity and charge-density wave in kagome metal CsV_3 Sb_5: Evidence from their evolutions with sample thickness, arXiv:2105.09248.

[30] Y. Song, T. Ying, X. Chen, X. Han, X. Wu, A. P. Schnyder, Y. Huang, J. G. Guo, and X. Chen, Competition of Superconductivity and Charge Density Wave in Selective Oxidized CsV_3 Sb_5 Thin Flakes, Phys. Rev. Lett. **127**, 237001 (2021).

[31] G. Xu, B. Lian, P. Tang, X. L. Qi, and S. C. Zhang, Topological Superconductivity on The Surface of Fe-Based Superconductors, Phys. Rev. Lett. **117**, 047001 (2016).

[32] W. Liu, L. Cao, S. Zhu, L. Kong, G. Wang, M. Papaj, P. Zhang, Y. B. Liu, H. Chen, G. Li, F. Yang, T. Kondo, S. Du, G. H. Cao, S. Shin, L. Fu, Z. Yin, H. J. Gao, and H. Ding, A new Majorana platform in an Fe-As bilayer superconductor, Nat. Commun. **11**, 5688 (2020).

[33] L. Kong, L. Cao, S. Zhu, M. Papaj, G. Dai, G. Li, P. Fan, W. Liu, F. Yang, X. Wang, S. Du, C. Jin, L. Fu, H. J. Gao, and H. Ding, Majorana zero modes in impurity-assisted vortex of LiFeAs superconductor, Nat. Commun. **12**, 4146 (2021).

[34] Y. Yuan, J. Pan, X. Wang, Y. Fang, C. Song, L. Wang, K. He, X. Ma, H. Zhang, F. Huang, W. Li, and Q.-K. Xue, Evidence of anisotropic Majorana bound states in 2M-WS_2, Nat. Phys. **15**, 1046 (2019).

[35] J. Y. You, B. Gu, G. Su, and Y. P. Feng, Emergent kagome electrides, J. Am. Chem. Soc. **144**, 5527 (2022).

[36] X.-W. Yi, Z.-W. Liao, J.-Y. You, B. Gu, and G. Su, Topological superconductivity and large spin Hall effect in the kagome family Ti_6X_4 (X = Bi, Sb, Pb, Tl, In), iScience, 105813 (2022).

[37] See Supplemental Material at http://link.aps.org/supplemental/10.1103/PhysRevB.106.L220505 for S1. Workflow for searching new structures; S2. Stable AB_3C_5 members; S3. Calculation methods; S4. Band structures, phonon spectrum, and Fermi surface; S5. Magnetic properties of $CsTi_3Pb_5$ and $RbCr_3Te_5$; S6. Possible CDW phases; S7. Topological surface states and Z_2 index, which includes Refs. [1,7,11,48–60].

[38] H. Tan, Y. Liu, Z. Wang, and B. Yan, Charge Density Waves and Electronic Properties of Superconducting Kagome Metals, Phys. Rev. Lett. **127**, 046401 (2021).

[39] L. Fu and C. L. Kane, Topological insulators with inversion symmetry, Phys. Rev. B **76**, 045302 (2007).

[40] B. R. Ortiz, S. M. L. Teicher, L. Kautzsch, P. M. Sarte, N. Ratcliff, J. Harter, J. P. C. Ruff, R. Seshadri, and S. D. Wilson, Fermi Surface Mapping and the Nature of Charge-Density-Wave Order in the Kagome Superconductor CsV_3 Sb_5, Phys. Rev. X **11**, 041030 (2021).

[41] L. Fu and E. Berg, Odd-parity Topological Superconductors: Theory and Application to $Cu_xBi_2Se_3$, Phys. Rev. Lett. **105**, 097001 (2010).

[42] Z. Wang, P. Zhang, G. Xu, L. K. Zeng, H. Miao, X. Xu, T. Qian, H. Weng, P. Richard, A. V. Fedorov, H. Ding, X. Dai, and Z. Fang, Topological nature of the $FeSe_{0.5}Te_{0.5}$ superconductor, Phys. Rev. B **92**, 115119 (2015).

[43] T. Sato, Y. Tanaka, K. Nakayama, S. Souma, T. Takahashi, S. Sasaki, Z. Ren, A. A. Taskin, K. Segawa, and Y. Ando, Fermiology of the Strongly Spin-Orbit Coupled Superconductor $Sn_{1-x}In_xTe$: Implications for Topological Superconductivity, Phys. Rev. Lett. **110**, 206804 (2013).

[44] J.-Y. You, B. Gu, G. Su, and Y. P. Feng, Two-dimensional topological superconductivity candidate in a van der Waals layered material, Phys. Rev. B **103**, 104503 (2021).

[45] Z. Zhang, J.-Y. You, B. Gu, and G. Su, Emergent topological superconductivity in bi-intercalated van der Waals layered $SiTe_2$, Phys. Rev. B **106**, 174519 (2022).

[46] S. Peng, Y. Han, G. Pokharel, J. Shen, Z. Li, M. Hashimoto, D. Lu, B. R. Ortiz, Y. Luo, H. Li, M. Guo, B. Wang, S. Cui, Z. Sun, Z. Qiao, S. D. Wilson, and J. He, Realizing Kagome Band Structure in Two-Dimensional Kagome Surface States of RV_6 Sn_6 (R = Gd, Ho), Phys. Rev. Lett. **127**, 266401 (2021).

[47] G. Pokharel, S. M. L. Teicher, B. R. Ortiz, P. M. Sarte, G. Wu, S. Peng, J. He, R. Seshadri, and S. D. Wilson, Electronic properties of the topological kagome metals YV_6 Sn_6 and GdV_6 Sn_6, Phys. Rev. B **104**, 235139 (2021).

[48] C. Mu, Q. Yin, Z. Tu, C. Gong, H. Lei, Z. Li, and J. Luo, S-wave superconductivity in kagome metal CsV_3 Sb_5 revealed by $^{121/123}$Sb NQR and ^{51}V NMR measurements, Chin. Phys. Lett. **38**, 077402 (2021).

[49] Z. Zhang, Z. Chen, Y. Zhou, Y. Yuan, S. Wang, J. Wang, H. Yang, C. An, L. Zhang, X. Zhu, Y. Zhou, X. Chen, J. Zhou, and Z. Yang, Pressure-induced reemergence of superconductivity in the topological kagome metal CsV_3 Sb_5, Phys. Rev. B **103**, 224513 (2021).

[50] P. E. Blöchl, Projector augmented-wave method, Phys. Rev. B **50**, 17953 (1994).

[51] G. Kresse and J. Furthmüller, Efficient iterative schemes for *ab initio* total-energy calculations using a plane-wave basis set, Phys. Rev. B **54**, 11169 (1996).

[52] J. P. Perdew, K. Burke, and M. Ernzerhof, Generalized Gradient Approximation Made Simple, Phys. Rev. Lett. **77**, 3865 (1996).

[53] A. Togo and I. Tanaka, First principles phonon calculations in materials science, Scr. Mater. **108**, 1 (2015).

[54] A. A. Mostofi, J. R. Yates, G. Pizzi, Y.-S. Lee, I. Souza, D. Vanderbilt, and N. Marzari, An updated version of WANNIER90: A tool for obtaining maximally-localized Wannier functions, Comput. Phys. Commun. **185**, 2309 (2014).

[55] M. P. L. Sancho, J. M. L. Sancho, J. M. L. Sancho, and J. Rubio, Highly convergent schemes for the calculation of bulk and surface Green functions, J. Phys. F: Met. Phys. **15**, 851 (1985).

[56] M. G. Vergniory, L. Elcoro, C. Felser, N. Regnault, B. A. Bernevig, and Z. Wang, A complete catalogue of high-quality topological materials, Nature (London) **566**, 480 (2019).

[57] W. L. McMillan, Transition temperature of strong-coupled superconductors, Phys. Rev. **167**, 331 (1968).

[58] P. B. Allen and R. C. Dynes, Transition temperature of strong-coupled superconductors reanalyzed, Phys. Rev. B **12**, 905 (1975).

[59] M. Kang, S. Fang, J.-K. Kim, B. R. Ortiz, S. H. Ryu, J. Kim, J. Yoo, G. Sangiovanni, D. Di Sante, B.-G. Park, C. Jozwiak, A. Bostwick, E. Rotenberg, E. Kaxiras, S. D. Wilson, J.-H. Park, and R. Comin, Twofold Van Hove singularity and origin of charge order in topological kagome superconductor CsV_3Sb_5, Nat. Phys. **18**, 301 (2022).

[60] U. Wolff, Collective Monte Carlo Updating for Spin Systems, Phys. Rev. Lett. **62**, 361 (1989).